Smart Structures and Systems, *Vol. 34, No. 1 (2024) 25-32*
https://doi.org/10.12989/sss.2024.34.1.025

Investigation of characteristic values in TDR waveform using SHapley Additive exPlanations (SHAP) for dielectric constant estimation during curing time

Won-Taek Hong [1a], WooJin Han [2b], Yong-Hoon Byun [3c] and Hyung-Koo Yoon*[4]

[1] *Department of Civil & Environmental Engineering, Gachon University, 1342, Seongnam-daero, Sujeong-gu, Seongnam-si, Gyeonggi-do, 13120, Republic of Korea*
[2] *School of Civil, Environmental and Architectural Engineering, Korea University, 145 Anam-ro, Seongbuk-gu, Seoul, 02841, Republic of Korea*
[3] *Department of Agricultural Civil Engineering, Kyungpook National University, 80 Daehak-ro, Buk-gu, Daegu, 41566, Republic of Korea*
[4] *Department of Construction and Disaster Prevention Engineering, Daejeon University, 62, Daehak-ro, Dong-gu, Daejeon, 34520, Republic of Korea*

(*Received May 7, 2024, Revised August 13, 2024, Accepted August 20, 2024*)

Abstract. As materials cure, the internal electrical flow changes, leading to variations in the dielectric constant over time. This study aims to assess the impact of voltage values extracted from time domain reflectometry (TDR) waveforms, measured during the curing of materials, on predicting the dielectric constant. The experiments are conducted over a curing period ranging from 60 to 8640 minutes, with 30 TDR trials. From the measured waveforms, values of V_0, V_1, V_2, V_f, and Δt are deduced. Additionally, curing time is included as an input variable. Groups A and B are distinguished based on the presence or absence of Δt, indicating a physical relationship between Δt and the dielectric constant. The dielectric constant is set as the output variable. The SHapley Additive exPlanations (SHAP) algorithm is applied to the compiled data. The results indicate that Δt and V_1 are the most influential input variables in both Group-A and Group-B. The study also presents the distribution of SHAP values and interacts SHAP values to infer the interrelationships among the input variables. To validate the reliability of these findings, the partial dependence (PD) algorithm is applied to estimate the marginal effects of each input variable, with outcomes closely aligning with those of the SHAP algorithm. This research suggests that understanding the contributions and proportional relationships of each input variable can aid in interpreting the relationships among various material properties.

Keywords: curing time; feature contribution; partial dependence (PD) algorithm; SHapley Additive exPlanations (SHAP) algorithm; time domain reflectometry (TDR)

1. Introduction

As construction materials cure, physical properties change with time, and those changes can be adopted to evaluate the serviceability of the infrastructures (Lim *et al*. 2021, Pei *et al*. 2016). Dielectric constant is known to be one of the properties that changes most sensitively to the changes in moisture and chemical components of construction materials, that may occur during the curing process (Piladaeng *et al*. 2016). Time domain reflectometry (TDR) is an effective method to estimate the dielectric properties of testing materials (Topp *et al*. 1980), and its ability to monitor the changes in dielectric properties has been demonstrated during the humidifying and dehumidifying process of a multi-phase material (Hong *et al*. 2016). Conventionally, the TDR system has been used to evaluate the volumetric water contents of the soils based on the velocity of electromagnetic wave propagating along the TDR probe in contact with the soils (Noborio *et al*. 1996). However, the application of TDR system was limited to laboratory tests and ground surface due to the problems with the TDR probe consisting of slender electrodes. To apply the TDR system to the subsurface, a modular penetration type TDR probe was developed, and the modularization technique was also adopted to install the TDR probe on the side of a cell used in the laboratory tests (Hong *et al*. 2022, Lee *et al*. 2018).

Although the studies and developments of TDR probes to apply the TDR system to the various experimental conditions have been conducted, a separate analysis procedure is required to determine the dielectric properties from the waveforms obtained from the TDR system using both standard and modular probes, which declines the time efficiency in analyzing the TDR waveforms. Therefore, a study on an analysis method to intuitively estimate the dielectric properties of the testing material based on the characteristic values that appear in the TDR waveform is required. In addition, investigation of influential levels of the characteristic values on the dielectric properties is necessary to reasonably estimate the dielectric constant of the testing material.

*Corresponding author, Ph.D., Associate Professor,
E-mail: hyungkoo@dju.ac.kr
[a] Ph.D., Assistant Professor
[b] Ph.D., Research Professor
[c] Ph.D., Associate Professor

ISSN: 1738-1584 (Print), 1738-1991 (Online)

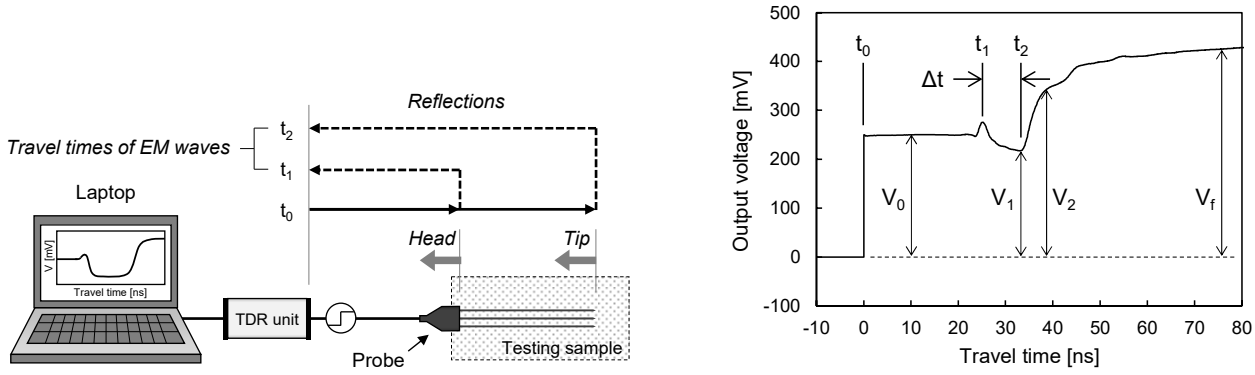

(a) TDR measurement system (b) Typical TDR waveform

Fig. 1 Time domain reflectometry (TDR)

Machine learning is increasingly applied across various engineering fields, leveraging the characteristics of measured data to predict the future behavior of subjects or to classify among similar datasets, thus assessing their mutual impacts (Byun *et al*. 2023, Mondal *et al*. 2023, Wang *et al*. 2023). The algorithms developed are chosen and utilized according to the user's objectives, with deep neural networks being the most commonly employed for regression and prediction tasks (Bang *et al*. 2023, Lin *et al*. 2023, Samadi *et al*. 2023). These algorithms use multiple layers of nodes between input and output variables to enhance output reliability (Min *et al*. 2023, Park *et al*. 2023). In addition to the number of nodes, fine-tuning hyperparameters related to weights and backpropagation also serves to improve reliability (Doan 2023, Zivari *et al*. 2023). However, despite these adjustments, results can sometimes plateau in terms of reliability (Zamani *et al*. 2023). To address this issue, it is crucial to reassess whether the input variables have been appropriately selected for deriving the output. Exploring each physical quantity of the input variables through a trial-and-error method poses a significant challenge. To surmount this, the SHapley Additive exPlanations (SHAP) model, a component of Explainable AI (XAI) algorithms, has been introduced (Alabi *et al*. 2023, Zhang *et al*. 2023). It offers the benefit of delineating the extent to which input variables influence the output and determining whether these influences are direct or inverse, thereby facilitating the selection of input variables that yield meaningful results through proportional relationships (Panda *et al*. 2023). Furthermore, it enables assessments based on specific input variable values; if acquiring a particular input variable is difficult, measuring data only within certain influential ranges can still produce excellent outcomes. This algorithm has been employed in numerous studies to discard unnecessary variables and boost the reliability of predictions via essential variables (Kim and Yoon 2023). Consequently, this research utilized the SHAP algorithm to explore the correlation in predicting the dielectric constant using various physical properties derived from time domain reflectometry (TDR) waveforms.

The paper starts with explanations of the foundational theories on time domain reflectometry (TDR) and the SHapley Additive exPlanations (SHAP) algorithm, followed by a description of the experimental methodology for measuring TDR waveforms. Key physical properties were identified and extracted from the measured TDR waveforms to analyze each input variable's contribution to predicting the dielectric constant, with a summary of the findings presented. Ultimately, the reliability of the results obtained through the SHAP method was validated by employing the partial dependence plot method.

2. Background theory

2.1 Time domain reflectometry

Time domain reflectometry (TDR) system is composed of TDR unit and waveguide including a coaxial cable and a TDR probe as shown in Fig. 1(a). The TDR probe consists of three electrodes; core electrode and two outer electrodes are connected to the core and outer conductors of coaxial cable. A step function of electromagnetic (EM) wave transmitted from TDR unit propagates along the waveguide and partially reflected along the entire path of the waveguide (Noborio *et al*. 1996). Especially, comparatively large energies of EM wave are reflected from the head and tip of the probe where EM impedance significantly changes within the waveguide. The transmitted and reflected EM waves are recorded as voltage with time, which is known as TDR waveform. A typical TDR waveform measured in a soil sample is shown in Fig. 1(b). The transmission time of EM wave (t_0) is set to 0, and the travel times of EM wave reflected from head and tip of the probe are defined as t_1 and t_2, respectively.

The TDR waveform can vary according to the specifications of TDR unit and probe and types of testing sample, and the characteristic values representing the TDR waveform are V_0, V_1, V_2, V_f, and Δt (Yanuka *et al*. 1988, Zegelin *et al*. 1989) as indicated in Figure 1(b). V_0 is the initial amplitude of the step function transmitted from TDR unit, V_1 and V_2 are the signal amplitudes at the beginning and end of reflection of the EM wave at the tip of the TDR probe, respectively, V_f is the signal amplitude that converges after a sufficient measurement time has elapsed, and Δt is the round trip travel time of EM wave in the TDR probe, which corresponds to the time difference between t_1 and t_2.

2.2 SHapley Additive exPlanations (SHAP) algorithm

The SHAP algorithm falls under the category of Explainable AI (XAI) algorithms and is employed to assess the contribution of each individual input variable by considering the characteristics of all the input variables collectively (Al-Swaidani *et al*. 2024, Cakiroglu *et al*. 2024, Vimbi *et al*. 2024). It evaluates how much each input variable contributes to the output and determines the shapley value for each input variable (Raihan *et al*. 2023). Previously, the importance of input variables was calculated using the random forest algorithm, which selects them through a bagging method (Min and Yoon 2021). However, this method is limited in that it only compares changes in the output value based on the presence or absence of randomly selected input variables, without establishing a coalition among the input values. In contrast, the SHAP algorithm, which is grounded in game theory, calculates the shapley value (φ) by examining the relationships among input variables, as illustrated in Eq. (1). Therefore, the SHAP algorithm offers the advantage of enabling a more precise determination of whether the relationship between input and output data is direct or inverse.

$$\varphi_n = \sum_{S \subseteq N/(i)} |S|!\,(n-1 - |S|)!\,[function(S \cup (i) - f(S)] \quad (1)$$

where N represents all features of the input data, and S denotes the selected data among the input data. The term function refers to the algorithm used to predict the output value from the input data, and n signifies the number of data points.

3. Experiment

3.1 Experimental process

To obtain TDR waveforms with curing time of construction materials, cement paste was prepared by mixing rapid hardening cement and water with a water to cement ratio of 45%. In addition, 60 grams of organic retarder was added to the cement paste per 10 kilograms of cement in order to obtain a sufficient number of TDR signals. The mixed cement paste was poured into a mold with a length, width, and height of 950 mm, 80 mm, and 80 mm, respectively, and three electrodes with a length and diameter of 950 mm and 2.5 mm are installed in the middle of the mold to configure a TDR probe. For the mixed and poured cement paste, a total number of 30 TDR waveforms were obtained with curing time from 60 to 8640 minutes: 60~360 minutes (30 minutes interval), 360~720 minutes (60 minutes interval), 720~1440 minutes (180 minutes interval), 1440~2160 minutes (360 minutes interval), 2160~5760 minutes (720 minutes interval), and 5760~8640 minutes (1440 minutes interval). Note that 64 signals were stacked to remove external random noises during each measurement.

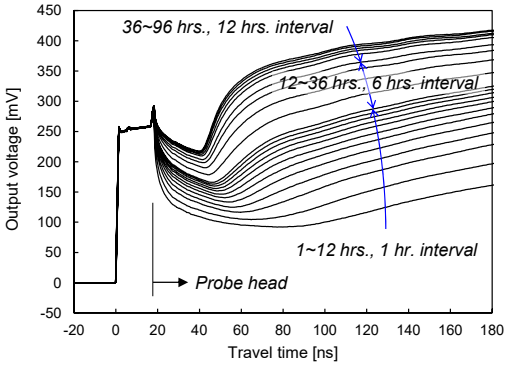

Fig. 2 TDR waveforms with curing time

3.2 Experimental results

TDR waveforms measured at the curing times of 1~12 hours (1 hour interval), 12~36 hours (6 hours interval), and 36~96 hours (12 hours interval) are selectively plotted in Fig. 2. The changes in signal amplitude at the probe head are significantly large at the early stage of curing time because the freshly mixed cement paste is strongly alkaline with a high electrical conductance, which results in large difference in EM impedances at the probe head. As the curing time passes, signal amplitude increases with changes in signal amplitude at the probe head decrease so that the characteristic values of V_1, V_2, and V_f increase with curing time.

Travel time of EM wave in the probe (Δt) is longer at the early stages of curing and gradually decreases with curing time. It has been reported that the uncured cementitious materials have very large dielectric constant and the dielectric constant decreases with curing time due to the results of hydration process. Because the velocity of EM wave is inversely proportional to the square root of dielectric constant, EM wave velocity in the cement paste at the early stage of curing time is slower than that in the sufficiently cured cement paste.

4. Feature contribution

4.1 SHAP algorithm

In this study, the SHAP algorithm, as previously outlined, was employed to determine the correlations among various input properties. The input variables were established as V_0, V_1, V_2, V_f, and Δt, all derived from the TDR waveform. Additionally, to account for variations in output values over the material's curing period, curing time was incorporated as another input variable. The dielectric constant was chosen as the output variable, with a database constructed following its calculation based on the TDR waveform's reflection time and the characteristics of the TDR sensor. A total of 30 data points were used, corresponding to the 30 TDR waveforms measured across different curing times. Given the physical correlation between the dielectric constant and Δt, SHAP analysis indicated that the Δt term might exhibit significantly greater importance compared to other input properties. To avoid an

overemphasis on Δt's importance, it was excluded from the input property dataset, and its association with the dielectric constant was further analyzed. Consequently, the input data were categorized into two groups: Group-A, comprising V_0, V_1, V_2, V_f, curing time, and Δt; and Group-B, consisting of five physical quantities excluding Δt. The dielectric constant remained the designated output variable for both groups.

4.2 Mean SHAP value

To explore feature contributions, the SHAP algorithm was employed, revealing correlations between input properties and the dielectric constant for both Group-A and Group-B. The predictive model utilized was the random forest, with the estimator and depth settings at 1000 and 1300, respectively. These results are concisely summarized in Fig. 3, where the calculated SHAP values are presented in absolute terms. A higher SHAP value in this figure indicates a stronger contribution to determining the output variable. As anticipated, Group-A's findings highlight Δt's significantly larger impact, with a SHAP value of 4.68, in contrast to other factors. This outcome is expected, considering the role of Δt in converting the dielectric constant, which also indirectly validates the SHAP results' reliability. The SHAP values for V_2 and V_f were notably high at 2.19 and 2.03, respectively, underscoring their importance. Notably, the curing time exhibited a higher SHAP value than the TDR waveform inputs V_0 and V_1, implying that variations in curing time — and consequently, the overall TDR waveform — somewhat influence the dielectric constant's fluctuation. Furthermore, V_0's lowest SHAP value at 1.44 among all input properties suggests its minimal contribution to the dielectric constant prediction. Conversely, Group-B, which omits Δt and includes only five input properties, yielded distinct outcomes from Group-A. Here, V_1 emerged as the most influential with a SHAP value of 3.21, followed by V_2, V_f, curing time, and V_0 with SHAP values of 3.19, 3.16, 2.96, and 2.54, respectively. Aside from V_1, the ranking of contributions for the remaining factors mirrors that of Group-A, yet the exclusion of Δt notably elevated V_1's prominence. Despite the ranking differences based on SHAP value sizes, V_1, V_2, and V_f displayed similar value ranges in both groups, indicating that, irrespective of input property types or experimental conditions, these factors consistently impact the dielectric constant estimation. Similar to its role in Group-A, V_0 was identified as the least influential input property on the output value.

4.3 Distributions of SHAP value

The results depicted in Fig. 3 allow us to identify the significant contributors within each group via SHAP values. Nonetheless, it is challenging to ascertain whether the effect of each input variable on the dielectric constant is directly or inversely proportional. To tackle this issue, the distribution of SHAP values was plotted across both negative and positive ranges, fully extending across the spectrum as illustrated in Fig. 4. In this figure, the dots represent the SHAP values calculated for each input property; red dots indicate a high contribution to the derivation of the dielectric constant, while blue dots suggest a relatively lower impact on predicting the output variable. In the results for Group-A, Δt's SHAP values show a wide span from -6 to +6, whereas the ranges for other input properties—V_2, V_f, curing time, and V_1—display distributions that are almost identical. V_1, however, presents a comparatively narrower range. As observed in Fig. 3, a broader range of SHAP values is associated with a higher contribution to the output variable. Additionally, Δt demonstrates that its contribution to feature analysis increases with positive SHAP values, revealing a directly proportional relationship, and shows inversely proportional characteristics at lower SHAP values. V_2, V_f, curing time, and V_1 exhibit opposite characteristics to Δt, suggesting an inversely proportional relationship in the prediction of the dielectric constant. In contrast, V_0 maintains a direct proportional relationship with the dielectric constant, akin to Δt. The outcomes for Group-B closely mirror those of Group-A, with the SHAP values for V_1, V_2, and V_f nearly spanning from -4 to +8. Curing time and V_0 are ranked subsequently. The patterns of direct and inverse proportionalities with the output variable appear in positions marked by red and blue, respectively, consistent with the Group-A findings. Therefore, V_1, V_2, V_f, and curing time exert a more substantial influence on estimating the dielectric constant when their values are lower, while V_0 plays a more significant role in influencing the output variable as its value increases.

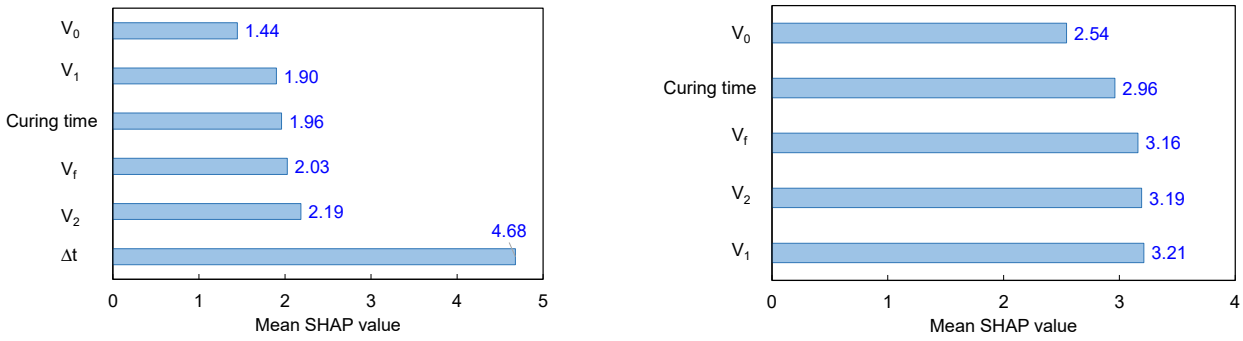

(a) All input variable (Group-A) (b) 5 kinds of input variables after removing Δt (Group-B)

Fig. 3 Mean SHAP values of each input variables

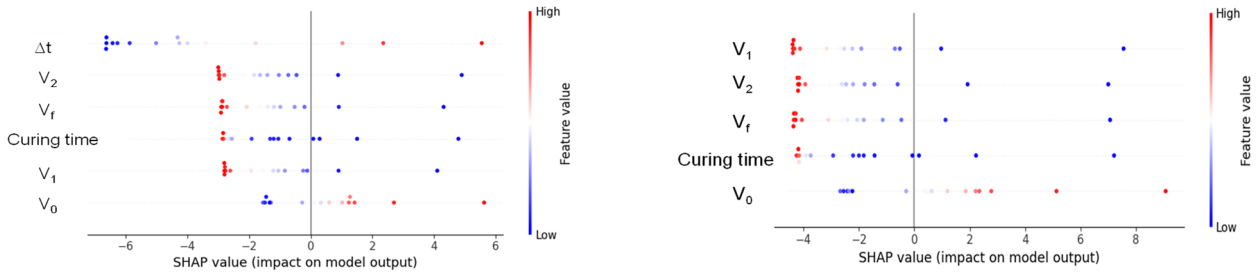

(a) All input variable (Group-A) (b) 5 kinds of input variables after removing Δt (Group-B)

Fig. 4 Distributions of SHAP values according to input variables

4.4 Interacted SHAP value

The insights derived from Figs. 3 and 4 indicate the feasibility of obtaining a relatively reliable estimate of the dielectric constant by focusing solely on the input properties with the most substantial contributions, albeit probabilistically. However, the phrase "to a certain extent" suggests that while incorporating all properties could naturally enhance the reliability of the dielectric constant's prediction, relying exclusively on the most significant contributors to approximate actual values introduces a degree of uncertainty. Consequently, examining the relationship between the most influential factor and other input variables allows for an understanding of the dominant factor's impact on the remaining properties, aiding in the decision-making process regarding their necessary extraction. In Group-A, the interplay among the input properties, anchored by Δt—identified as the most impactful contributor—is depicted in Fig. 5. This figure, which omits Δt, illustrates the behavioral trends of the five physical quantities, with red and blue denoting the impact spectrum as Δt values fluctuate. V_2, V_f, curing time, and V_1 exhibit a clear demarcation between red and blue, highlighting that color transitions occur at SHAP values nearing zero. Moreover, consistent with Fig. 4's findings, Δt, V_2, V_f, curing time, and V_1 demonstrate inversely proportional characteristics. The combined red and blue symbol distribution for V_0, however, suggests the difficulty in identifying a consistent trend with Δt variations, akin to the other input variables. A directly proportional relationship is notably present only around the values of approximately 249.8-249.9 mV, complicating uniform assessments of contribution to the output value. The analysis for Group-B, displayed in Fig. 6, focuses on V1 as the input property with the highest contribution. Curing time, V_f, and V_2 all manifest a direct proportional relationship with V_1, with turning points also emerging near SHAP values around zero. Therefore, as explored through Figs. 4 and 5, V_1, V_2, V_f, and curing time consistently show a direct proportional relationship. V_0, however, appears to exhibit no consistent pattern, as evidenced in Fig. 5. While Fig. 6 reveals shifts in red and blue symbols at junctures where the SHAP value is almost zero, the significant fluctuation in SHAP values poses challenges in generalizing the characteristics of feature contributions.

5. Discussion

In this study, input properties were divided into Group-A

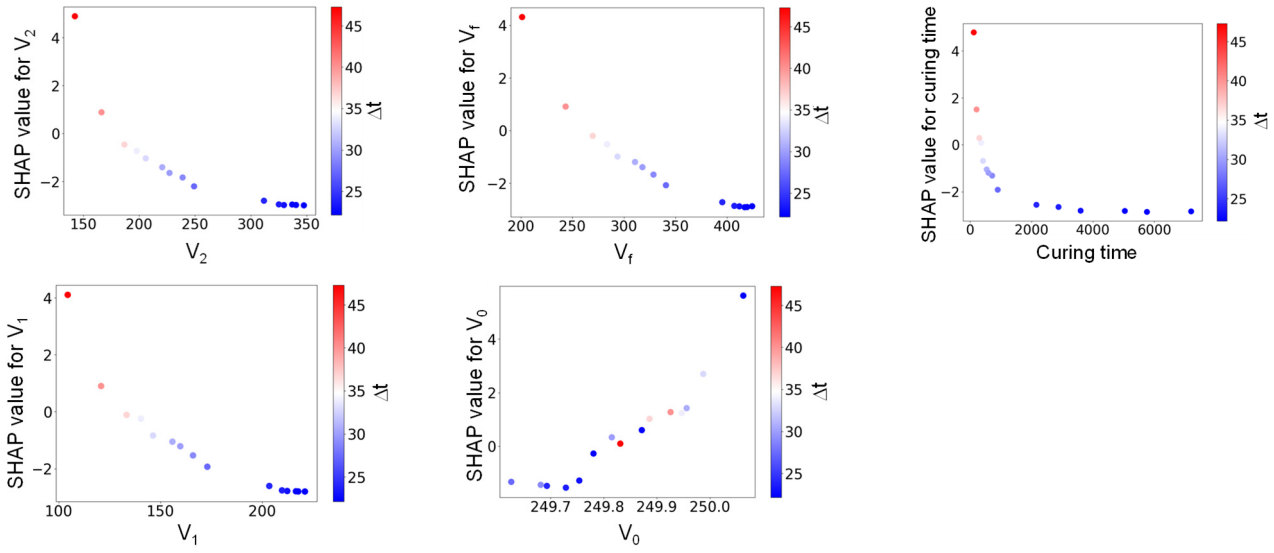

Fig. 5 Distribution of each input property and its corresponding SHAP value (Group-A). It also illustrates the interaction of each input property on Δt, the factor that has the most significant influence on the dielectric constant

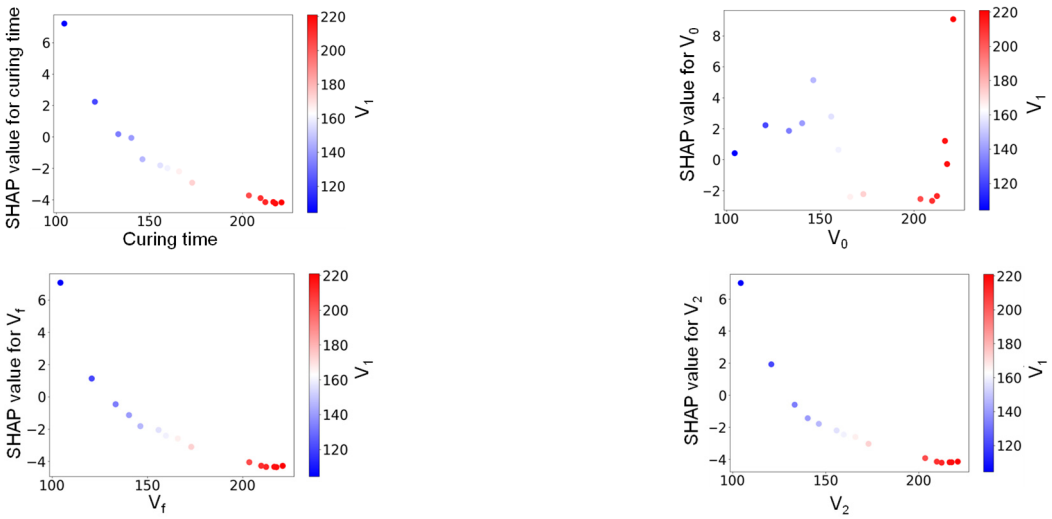

Fig. 6 Distribution of each input property (Group-B) and its corresponding SHAP value with interaction of each input property on V_1

(a) All input variable (Group-A)

(b) 5 kinds of input variables after removing Δt (Group-B)

Fig. 7 Partial dependence values with input variables

and Group-B to examine their relationships with the dielectric constant through SHAP values. The analysis revealed Δt and V_1 as the factors contributing most significantly in Group-A and Group-B, respectively. To delve deeper into the behavior informed by the range and distribution of SHAP values, interactions among the variables were also explored. To validate these findings, results from a partial dependence (PD) analysis were presented in Fig. 7. Unlike SHAP, which depicts the degree of contribution through the interconnectivity of factors, the PD algorithm assesses the marginal effect of individual factors on the outcome, providing a marginal distribution by varying one variable at a time while holding others constant (Molnar *et al.* 2023, Siqueira *et al.* 2024). PD values for both Group-A and Group-B were analyzed, with differing value ranges of each input property leading to normalization to a 0-1 scale for uniform comparison.Curing time, exhibiting a wide range of input values, showed PD values across the entire 0-1 spectrum after normalization, indicating its impact on the dielectric constant at normalized values below 0.1. This finding aligns with that of Fig. 5, demonstrating that the influence of curing time on dielectric constant predictions diminishes as its value increases. Conversely, as normalized values for Δt increase, corresponding PD values rise, suggesting its comparatively higher impact on the dielectric constant. V_1, V_2, and V_f showed an inversely proportional relationship between normalized values and PD values, whereas V_0's normalized value range was minimal, displaying results nearly converging to 1 on the x-axis. These PD outcomes mirror the behaviors identified through SHAP in Figs. 3, 4, and 5, with Δt exerting the greatest influence and V_0 the least in predicting the dielectric constant. Group-B's PD values similarly reflected those of Group-A, with curing time exhibiting an inversely proportional behavior and minimal impact beyond a normalized value of 0.1. Although V_1, V_2, and V_f in Group-B shared similar normalized values with Group-A, the computed PD values were notably higher. This suggests a redistribution of the focused contribution from Δt in Group-A to other factors in Group-B, resulting in increased PD values. Like in Group-A, V_0 showed the smallest normalized values and a narrow range of PD values, indicating the least contribution to dielectric constant predictions.

The PD outcomes in Fig. 7, closely resembling the SHAP results from Figs. 3, 4, 5, and 6, reinforce the reliability of evaluating the impact of variables extracted from TDR waveforms on the dielectric constant in relation to curing time. Although Δt and V_1 are highlighted as primary contributors in both groups, this does not

necessarily imply that predictions based solely on these factors would be reliably accurate. The findings stress the need to consider all variables within Groups A and B for precise estimation of the dielectric constant, given the interactive effects of input variables. Nevertheless, should accurate measurements become challenging due to waveform measurement errors or changes in the experimental environment, ensuring the precise extraction of Δt and V_1 as essential factors becomes crucial.

TDR measurement involves artificially creating an electric field and obtaining voltage profiles based on this field, making it suitable for understanding the properties of various media, not just concrete. In this study, the changing voltage as the concrete cured was designated as an independent variable to monitor changes in the concrete's properties. Although this technique was applied specifically to concrete, the method presented is considered to have potential applications across a range of materials.

6. Conclusions

In this research, changes in the internal state of materials during curing led to variations in the dielectric constant. The aim was to analyze the contribution of various input variables to estimating the dielectric constant. For this purpose, the SHapley Additive exPlanations (SHAP) algorithm, a component of Explainable AI (XAI) methodologies, was employed. The principal findings are summarized as follows:

- Waveforms were captured using time domain reflectometry over a period ranging from 60 to 8640 minutes, resulting in a total of 30 measured signals. From these signals, V_0, V_1, V_2, V_f, and Δt were extracted and designated as input variables. Curing time was also included as an additional input factor, and the output variable was specified as the dielectric constant. Owing to the physical correlation between Δt and the dielectric constant, the dataset was segmented into groups A and B, based on the presence or absence of Δt, to apply XAI techniques.
- The SHAP algorithm was utilized to present the mean SHAP values, enabling the evaluation of each input variable's contribution. This was accompanied by the distribution of SHAP values to deduce the interrelationships among the input variables. The analysis revealed that Δt and V1 significantly influence the prediction of the dielectric constant in both groups A and B. Consequently, Interacted SHAP values were depicted to investigate the connections between the remaining input variables, thus discerning the proportional and inversely proportional relationship between the dielectric constant and the properties with the highest contributions.
- To corroborate the SHAP findings' credibility, the partial dependence (PD) algorithm was applied to estimate the PD values for each input property. The analysis of PD values relative to normalized input values demonstrated behaviors closely mirroring those observed with SHAP, thereby affirming the study's reliability.

Acknowledgments

This work was supported by the National Research Foundation of Korea (NRF) grant funded by the Korea government (MSIT) (NRF-2020R1A2C2012113), (2022R1A4A3029737).

References

Alabi, R.O., Elmusrati, M., Leivo, I., Almangush, A. and Mäkitie, A.A. (2023), "Machine learning explainability in nasopharyngeal cancer survival using LIME and SHAP", *Scientif. Reports*, **13**(1), 8984. https://doi.org/10.1038/s41598-023-35795-0

Al-Swaidani, A.M., Meziab, A., Khwies, W. T., Al-Bali, M. and Lala, T. (2024), "Building MLR, ANN and FL models to predict the strength of problematic clayey soil stabilized with a combination of nano lime and nano pozzolan of natural sources for pavement construction", *Int. J. Geo-Eng.*, **15**(1), 2. https://doi.org/10.1186/s40703-023-00201-1

Bang, H., Yu, B. and Jeon, H. (2023), "Assembly performance evaluation method for prefabricated steel structures using deep learning and k-nearest neighbors", *Smart Struct. Syst.*, *Int. J.*, **32**(2), 111-121. https://doi.org/10.12989/sss.2023.32.2.111

Byun, N., Lee, J., Lee, K. and Kang, Y.J. (2023), "Extended artificial neural network for estimating the global response of a cable-stayed bridge based on limited multi-response data", *Smart Struct. Syst.*, *Int. J.*, **32**(4), 235-251. https://doi.org/10.12989/sss.2023.32.4.235

Cakiroglu, C., Demir, S., Ozdemir, M.H., Aylak, B.L., Sariisik, G. and Abualigah, L. (2024), "Data-driven interpretable ensemble learning methods for the prediction of wind turbine power incorporating SHAP analysis", *Expert Syst. Applicat.*, **237**, 121464. https://doi.org/10.1016/j.eswa.2023.121464

Doan, N.S. (2023), "Reliability analysis and uncertainty quantification of clay and sand slopes stability evaluated by Fellenius and Bishop's simplified methods", *Int. J. Geo-Eng.*, **14**(1), 22. https://doi.org/10.1186/s40703-023-00200-2

Hong, W.T., Jung, Y.S., Kang, S. and Lee, J.S. (2016), "Estimation of soil-water characteristic curves in multiple-cycles using membrane and TDR system", *Materials*, **9**(12), 1019. https://doi.org/10.3390/ma9121019

Hong, W.T., Lee, J.S., Lee, D. and Yoon, H.K. (2022), "Estimation of bulk electrical conductivity in saline medium with contaminated lead solution through TDR coupled with machine learning", *Process Safe. Environ. Protect.*, **161**, 58-66. https://doi.org/10.1016/j.psep.2022.03.018

Jabeur, S.B., Mefteh-Wali, S. and Viviani, J.L. (2024), "Forecasting gold price with the XGBoost algorithm and SHAP interaction values", *Annals Operat. Res.*, **334**(1), 679-699. https://doi.org/10.1007/s10479-021-04187-w

Kim, S. and Yoon, H.K. (2023), "Application of classification coupled with PCA and SMOTE, for obtaining safety factor of landslide based on HRA", *Bull. Eng. Geol. Environ.*, **82**(10), 381. https://doi.org/10.1007/s10064-023-03403-0

Lee, J.S., Hong, W.T., Park, K., Hong, S.S., Lee, S.H. and Byun, Y.H. (2018), "Evaluation of water content in an active layer using penetration-type time domain reflectometry", *Appl. Sci.*, **8**(6), 935. https://doi.org/10.3390/app8060935

Lim, Y.Y., Smith, S.T., Padilla, R.V. and Soh, C.K. (2021), "Monitoring of concrete curing using the electromechanical impedance technique: Review and path forward", *Struct. Health*

Monitor., **20**(2), 604-636. https://doi.org/10.1177/1475921719893069

Lin, G., Zhang, Y., Cai, E., Zhao, T. and Li, Z. (2023), "An ensemble learning based Bayesian model updating approach for structural damage identification", *Smart Struct. Syst*., *Int. J*., **32**(1), 61-81. https://doi.org/10.12989/sss.2023.32.1.061

Min, D.H. and Yoon, H.K. (2021), "Suggestion for a new deterministic model coupled with machine learning techniques for landslide susceptibility mapping", *Scientif. Reports*, **11**(1), 1-24. https://doi.org/10.1038/s41598-021-86137-x

Min, D.H., Kim, Y., Kim, S. and Yoon, H.K. (2023), "Strategy of oversampling geotechnical parameters through geostatistical, SMOTE, and CTGAN methods for assessing susceptibility of landslide", *Landslides*, 1-17. https://doi.org/10.1007/s10346-023-02166-9

Molnar, C., König, G., Bischl, B. and Casalicchio, G. (2023), "Model-agnostic feature importance and effects with dependent features: a conditional subgroup approach", *Data Min. Knowled. Discov*., 1-39. https://doi.org/10.1007/s10618-022-00901-9

Mondal, T.G., Chou, J.Y., Fu, Y. and Mao, J. (2023), "A hybrid deep neural network compression approach enabling edge intelligence for data anomaly detection in smart structural health monitoring systems", *Smart Struct. Syst*., *Int. J*., **32**(3), 179-193. https://doi.org/10.12989/sss.2023.32.3.179

Noborio, K., McInnes, K.J. and Heilman, J.L. (1996), "Measurements of soil water content, heat capacity, and thermal conductivity with a single TDR probe1", *Soil Sci*., **161**(1), 22-28.

Panda, C., Mishra, A.K., Dash, A.K. and Nawab, H. (2023), "Predicting and explaining severity of road accident using artificial intelligence techniques, SHAP and feature analysis", *Int. J. Crashworth*., **28**(2), 186-201. https://doi.org/10.1080/13588265.2022.2074643

Park, J., Lee, J.S. and Yoon, H.K. (2023), "Geoacoustic and geophysical data-driven seafloor sediment classification through machine learning algorithms with property-centered oversampling techniques", *Comput.-Aided Civil Infrastr. Eng*., **39**(14), 2105-2121. https://doi.org/10.1111/mice.13126

Pei, J., Cai, J., Zou, D., Zhang, J., Li, R., Chen, X. and Jin, L. (2016), "Design and performance validation of high-performance cement paste as a grouting material for semi-flexible pavement", *Constr. Build. Mater*., **126**, 206-217. https://doi.org/10.1016/j.conbuildmat.2016.09.036

Piladaeng, N., Angkawisittpan, N. and Homwuttiwong, S. (2016), "Determination of relationship between dielectric properties, compressive strength, and age of concrete with rice husk ash using planar coaxial probe", *Measur. Sci. Rev*., **16**(1), 14. https://doi.org/10.1515/msr-2016-0003

Raihan, M.J., Khan, M.A.M., Kee, S.H. and Nahid, A.A. (2023), "Detection of the chronic kidney disease using XGBoost classifier and explaining the influence of the attributes on the model using SHAP", *Scientif. Reports*, **13**(1), 6263. https://doi.org/10.1038/s41598-023-33525-0

Samadi, H., Hassanpour, J. and Rostami, J. (2023), "Prediction of earth pressure balance for EPB-TBM using machine learning algorithms", *Int. J. Geo-Eng*., **14**(1), 21. https://doi.org/10.1186/s40703-023-00198-7

Siqueira, R.G., Moquedace, C.M., Fernandes-Filho, E.I., Schaefer, C.E., Francelino, M.R., Sacramento, I.F. and Michel, R.F. (2024), "Modelling and prediction of major soil chemical properties with Random Forest: Machine learning as tool to understand soil-environment relationships in Antarctica", *Catena*, **235**, 107677. https://doi.org/10.1016/j.catena.2023.107677

Topp, G.C., Davis, J.L. and Annan, A.P. (1980), "Electromagnetic determination of soil water content: Measurements in coaxial transmission lines", *Water Resour. Res*., **16**(3), 574-582. https://doi.org/10.1029/WR016i003p00574

Vimbi, V., Shaffi, N. and Mahmud, M. (2024), "Interpreting artificial intelligence models: a systematic review on the application of LIME and SHAP in Alzheimer's disease detection", *Brain Inform*., **11**(1), 10. https://doi.org/10.1186/s40708-024-00222-1

Wang, G., Wang, K.C., Zhang, A.A. and Yang, G. (2023), "A deep and multiscale network for pavement crack detection based on function-specific modules", *Smart Struct. Syst*., *Int. J*., **32**(3), 135-151. https://doi.org/10.12989/sss.2023.32.3.135

Yanuka, M., Topp, G.C., Zegelin, S. and Zebchuk, W.D. (1988), "Multiple reflection and attenuation of time domain reflectometry pulses: Theoretical considerations for applications to soil and water", *Water Resour. Res*., **24**(7), 939-944. https://doi.org/10.1029/WR024i007p00939

Zamani, S., Lajevardi, S.H., Yarivand, A. and Zeighami, E. (2023), "Experimental study of the behavior of square footing on reinforced sand with treated geotextile", *Int. J. Geo-Eng*., **14**(1), 19. https://doi.org/10.1186/s40703-023-00195-w

Zegelin, S.J., White, I. and Jenkins, D.R. (1989), "Improved field probes for soil water content and electrical conductivity measurement using time domain reflectometry", *Water Resour. Res*., **25**(11), 2367-2376. https://doi.org/10.1029/WR025i011p02367

Zhang, J., Ma, X., Zhang, J., Sun, D., Zhou, X., Mi, C. and Wen, H. (2023), "Insights into geospatial heterogeneity of landslide susceptibility based on the SHAP-XGBoost model", *J. Environ. Manag*., **332**, 117357. https://doi.org/10.1016/j.jenvman.2023.117357

Zivari, A., Siavoshnia, M. and Rezaei, H. (2023), "Effect of lime-rice husk ash on geotechnical properties of loess soil in Golestan province, Iran", *Int. J. Geo-Eng*., **14**(1), 20. https://doi.org/10.1186/s40703-023-00199-6